mater.scichina.com link.springer.com https://doi.org/10.1007/s40843-025-3735-x

Organic semiconductor blends: beyond Flory-Huggins theory

Yuying Wu and Ting Lei*

Organic electronics, such as organic solar cells (OSCs), doped organic field-effect transistors (OFETs), and organic thermoelectrics (OTEs), represent a class of devices that employ multiple organic materials, including conjugated polymer and small-molecules [1]. The performance and stability of such devices are closely related to the microscopic phase morphology of the active layer [2,3]. This morphology is determined by the thermodynamic phase behaviour of the mixture, which is traditionally described by Flory-Huggins (FH) theory and characterized by phase diagrams exhibiting upper critical solution temperature (UCST) behaviour [4]. In such diagrams, the components are miscible at high temperatures and undergo phase separation upon cooling (Fig. 1a, c). However, a recent study by Ade *et al.* [5] published in *Nature Materials* challenges this conventional perspective. Their work demonstrates that a significant number of polymer and small molecule blends exhibit complex re-entrant phase behaviour rather than simple UCST-type phase separation. This finding underscores the urgent need to extend thermodynamic models fundamentally beyond the framework of FH theory.

The research constructed temperature-composition (T-Φ) phase diagrams for 55 distinct blends, comprising ten different donor polymers and nine types of fullerene and non-fullerene (NF)-type small molecule acceptors (SMAs) with varied molecular structures. The binodal, which represents the boundary of miscibility, was determined in the polymer-rich region through time-of-flight secondary ion mass spectrometry (ToF-SIMS) analysis of polymer/SMA bilayer diffusion samples. It is noteworthy that nearly half of the studied systems deviate from simple UCST behaviour (Fig. 1g). Instead, they exhibit re-entrant phase behaviour, which can be categorized into two distinct types: hourglass (Fig. 1b, e) and looped (Fig. 1c, f). In these systems, blends that undergo phase separation at a certain temperature can become miscible again upon further heating or cooling, effectively "re-entering" the single-phase region. An intriguing finding is the correlation observed between the re-entrant transition temperature and the glass transition temperature (T_g) of the SMA (Fig. 1h), which strongly suggests a crucial role of configurational entropy and vitrification in collectively governing the phase behaviour.

The observation of such widespread re-entrant phase behaviour signals the breakdown of the classical FH model, which lacks the physical elements to account for this phenomenon. To address this limitation, they introduced a new physical model that integrates the lattice fluid (LF) model with the two-state bond (TSB) model, referred to as the LF-TSB model. The LF model incorporates compressibility and vacancies, allowing the equilibrium vacancy fraction ξ_{eq} to vary with temperature, pressure, and composition. This accounts for lower critical solution temperature (LCST) behaviour (i.e., phase separation upon heating) at high temperatures. The TSB model, originally proposed by Gibbs and DiMarzio [6], simulates the semiflexibility of polymer chains by treating the backbone bonds as existing in either a rigid (ground, A state) state or a flexible (excited, B state) state, with an energy difference of $\Delta\varepsilon_{i=A,B}$. This approach introduces a configurational entropy term that depends on the proportion of flexible bonds, which is sensitive to both the chemical structure of the blend and its proximity to the T_g.

The LF-TSB model successfully qualitatively reproduces all observed phase behaviours: UCST, hourglass, and looped. Calculations indicate that the LCST behaviour results from the greater favourability of accommodating vacancies in the pure state rather than in the mixture [7]. The hourglass shape originates from the merging of a low-temperature, FH-like UCST gap and a high-temperature LCST gap. In contrast, the looped behaviour is primarily entropy-driven. This behaviour emerges when a disparity in flexibility (or T_g) between components creates a scenario where maximizing configurational entropy favors phase separation at intermediate temperatures. The model identifies the monomer volume ratio (v^*_A/v^*_B) of the components as a key parameter governing the topology of the phase diagram. Furthermore, the authors carefully address the issue of vitrification by incorporating non-equilibrium thermodynamics to estimate the glass transition line, confirming that the experimentally observed re-entrant features occur in a temperature range where the equilibrium model remains valid.

This work propels the field beyond the simplified FH theory by providing an advanced and physically grounded theoretical framework capable of explaining previously anomalous experimental observations and predicting new phenomena. From a practical perspective, the type of phase diagram is directly correlated with device stability. Blends exhibiting a broad UCST gap, such as PM6:Y6 [8], possess a strong thermodynamic driving force for phase separation, resulting in their poor thermodynamic stability. In contrast, blends with a narrow hourglass miscibility gap, like PTB7-Th:EH-IDTBR (PTB7-Th: poly[4,8-bis(5-(2-ethylhexyl)thiophen-2-yl)benzo[1,2-*b*:4,5-*b*′]dithio-

Key Laboratory of Polymer Chemistry and Physics of Ministry of Education, School of Materials Science and Engineering, Peking University, Beijing 100871, China
* Corresponding author (email: Tinglei@pku.edu.cn)

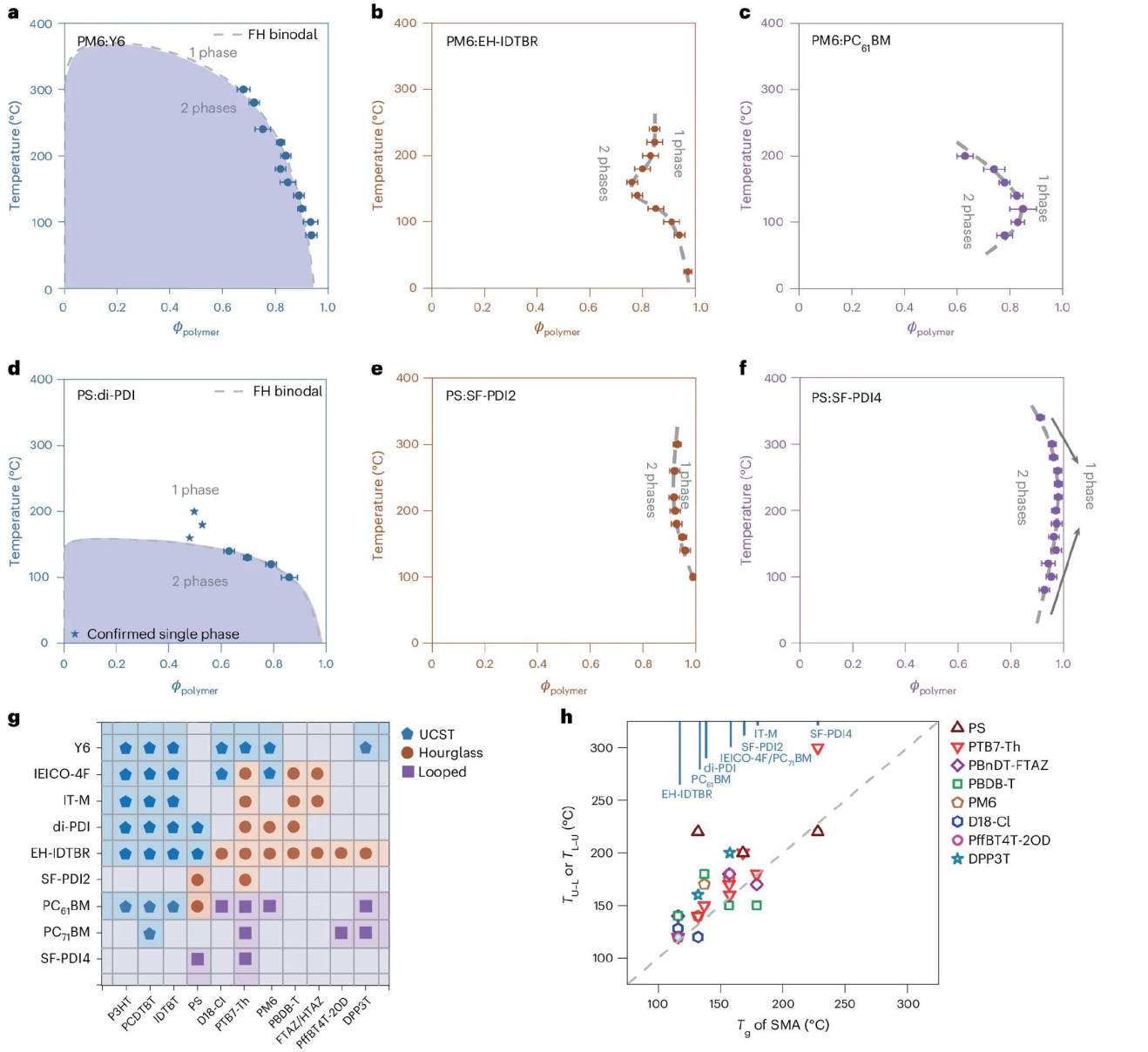

Figure 1 Phase diagrams of (a) PM6:Y6 (poly[(2,6-(4,8-bis(5-(2-ethylhexyl-3-fluoro)thiophen-2-yl)-benzo[1,2-*b*:4,5-*b*′]dithiophene))-*alt*-(5,5′-(1′,3′-di-2-thienyl-5′,7′-bis(2-ethylhexyl)benzo[1′,2′-*c*:4′,5′-*c*′]dithiophene-4,8-dione))]:2,2′-((2*Z*,2′*Z*)-((12,13-bis(2-ethylhexyl)-3,9-diundecyl-12,13-dihydro-[1,2,5]thiadiazolo[3,4-*e*]thieno[2,3:4,5]thieno[2′,3′:4,5]pyrrolo[3,2-*g*]thieno[2′,3′:4,5]thieno[3,2-*b*]indole-2,10-diyl)bis(methanylylidene))bis(5,6-difluoro-3-*oxo*-2,3-dihydro-1*H*-indene-2,1-diylidene))dimalononitrile), (b) PM6:EH-IDTBR (EH-IDTPR: (*Z*)-5-{[5-(15-{5-[(*Z*)-(3-ethyl-4-*oxo*-2-thioxo-1,3-thiazolidin-5-ylidene)methyl]-8-thia-7,9-diazabicyclo[4.3.0]nona-1(9),2,4,6-tetraen-2-yl}-9,9,18,18-tetrakis(2-ethylhexyl)-5,14-dithiapentacyclo[10.6.03,10.04,8.013,17]octadeca-1(12),2,4(8),6,10,13(17),15-heptaen-6-yl)-8-thia-7,9-diazabicyclo[4.3.0]nona-1(9),2,4,6-tetraen-2-yl]methylidene}-3-ethyl-2-thioxo-1,3-thiazolidin-4-one), (c) PM6:PC$_{61}$BM (poly[(2,6-(4,8-bis(5-(2-ethylhexyl-3-fluoro)thiophen-2-yl)-benzo[1,2-*b*:4,5-*b*′]dithiophene))-*alt*-(5,5′-(1′,3′-di-2-thienyl-5′,7′-bis(2-ethylhexyl)benzo[1′,2′-*c*:4′,5′-*c*′]dithiophene-4,8-dione))]:[6,6]-phenyl-C$_{61}$-butyric acid methyl ester), (d) PS:di-PDI (polystyrene:2,2′,9,9′-tetrakis(1-pentylhexyl)-[5,5′-bianthra[2,1,9-*def*:6,5,10-*d*′*e*′*f*′]diisoquinoline]-1,1′,3,3′,8,8′,10,10′-(2*H*,2′*H*,9*H*,9′*H*)-octone), (e) PS:SF-PDI2 (polystyrene:2,7′-di[*N*,*N*′-bis(2-octyl-dodecyl)-perylene-3,4,9,10-tetracarboxylic diimide]-9,9′-spirobi[9*H*-fluorene]), and (f) PS:SF-PDI4 (polystyrene:2,2′,7,7′-tetrakis[*N*,*N*′-bis(2-octyl-dodecyl)-perylene-3,4,9,10-tetracarboxylic diimide]-9,9′-spirobi[9*H*-fluorene]) as representative examples for UCST, hourglass, and looped, respectively. $\phi_{polymer}$ is the mean volume fraction of polymer in the blend. The dashed lines in (a) and (d) represent an empirical fit against the FH model. We note that the FH fits in (a) and (d) indicate that the SMA-rich boundary segments are close to $\phi_{polymer} \approx 0$. For the hourglass and looped ones, the SMA-rich boundary segments are expected to be close to $\phi_{polymer} \approx 0$ as well due to the asymmetry between the polymer and SMA. The grey dashed lines in (b, c) and (e, f) are a guide for the eye to delineate the polymer-rich boundary segment. The data represent the average from three different experiments with error bars from the statistics. (g) Overview of the phase diagram types for all 55 polymer:SMA systems. (h) Transition temperature T_{U-L} or T_{L-U} versus T_g correlation analysis, where T_{U-L} or T_{L-U} are denoted for the temperature switching from UCST to LCST in hourglass or the temperature switching from LCST to UCST in looped diagrams, respectively. T_{U-L} represents the critical temperature at which the system, during cooling, first transitions from the high-temperature upper single-phase region into the lower two-phase region. The definition of T_{U-L} is converse. Note: they used T_c (critical temperature) as a proxy for T_g for the material, namely IT-M, since its actual T_g is difficult to establish. Reproduced with permission from Ref. [5]. Copyright 2025, Nature Publishing Group.

phene-2,6-diyl-*alt*-(4-(2-ethylhexyl)-3-fluorothieno[3,4-*b*]thiophene-2-carboxylate-2,6-diyl)]) [9], demonstrate a suppressed driving force, thereby resulting in superior thermal stability. This understanding establishes new guidelines for designing stable OSCs. It indicates that in the selection or design of SMAs, we can rationally modulate molecular rigidity (to tailor T_g), side-chain architecture (to optimize the effective monomeric volume), and molecular symmetry (to harness configurational entropy), thereby guiding the formation of re-entrant phase diagrams to achieve the desired and stable microscopic phase morphology. Furthermore, it suggests innovative processing strategies, such as multi-step annealing across the re-entrant temperature zone, to trap beneficial morphological states.

While the LF-TSB model exhibits considerable potential, the practicality of its predictability and generalizability still faces some challenges. On one hand, the model introduces multiple new parameters (such as effective monomeric volume and flexing energy), but determining these parameters relies on fitting to experimental phase diagrams. For entirely new, unexplored blend systems, the ability to predict phase diagrams is constrained by the challenge of obtaining the necessary parameters accurately a priori. On the other hand, the model primarily focuses on the phase diagrams of the SMA and semiconducting polymer blends. Its applicability to other systems, such as polymer-polymer blends, amorphous small molecule-small molecule blends, or semiconducting polymer hydrogel systems [10], warrants further exploration.

Received 24 September 2025; accepted 30 September 2025; published online 1 December 2025

1 Jia H, Huang Z, Li P, *et al.* Engineering donor–acceptor conjugated polymers for high-performance and fast-response organic electrochemical transistors. J Mater Chem C, 2021, 9: 4927–4934
2 Ghasemi M, Hu H, Peng Z, *et al.* Delineation of thermodynamic and kinetic factors that control stability in non-fullerene organic solar cells. Joule, 2019, 3: 1328–1348
3 Zhu M, Li P, Li JL, *et al.* Molecular packing and film morphology control in organic electrochemical transistors. Mol Syst Des Eng, 2022, 7: 6–20
4 Ye L, Hu H, Ghasemi M, *et al.* Quantitative relations between interaction parameter, miscibility and function in organic solar cells. Nat Mater, 2018, 17: 253–260
5 Peng Z, Ghasemi M, Michels JJ, *et al.* Re-entrant phase behaviour of organic semiconductors. Nat Mater, 2025, doi: 10.1038/s41563-025-02348-x
6 Gibbs JH, DiMarzio EA. Nature of the glass transition and the glassy state. J Chem Phys, 1958, 28: 373–383
7 Lacombe RH, Sanchez IC. Statistical thermodynamics of fluid mixtures. J Phys Chem, 1976, 80: 2568–2580
8 Qin Y, Balar N, Peng Z, *et al.* The performance-stability conundrum of BTP-based organic solar cells. Joule, 2021, 5: 2129–2147
9 Zhang Z, Miao J, Ding Z, *et al.* Efficient and thermally stable organic solar cells based on small molecule donor and polymer acceptor. Nat Commun, 2019, 10: 3271
10 Li P, Sun W, Li J, *et al.* N-type semiconducting hydrogel. Science, 2024, 384: 557–563